ON EFFECTS OF INCREASING AMPLITUDE IN A BOUNDARY-LAYER SPOT

B. T. DODIA, R. G. A. BOWLES AND F. T. SMITH

Abstract. The boundary-layer spots involved here come from large-time theory and related computations on the Euler equations to cover the majority of the global properties of the spot disturbances, which are nonlinear, three-dimensional, and transitional rather than turbulent. The amplitude levels investigated are higher than those examined in detail previously and produce a new near-wall momentum contribution in the mean flow, initially close to the wing-tips of the spot. This enables the amplitude levels in the analysis to be raised successively, a process which gradually causes the wing-tip region to spread inwards. The process is accompanied by subtle increases in the induced phase variations. Among other things the work finds the details of how nonlinear effects grow from the wing-tips to eventually alter the entire trailing edge, and then the centre of the spot, in a strongly nonlinear fashion. Comparisons with earlier suggestions and with experiments are described at the end.

§1. *Introduction.* A recent special issue of JEM (Clark, Jones and LaGraff [1], Henningson, Johansson and Alfredsson [2], Seifert, Zilberman and Wyg-nanski [3], Shaikh and Gaster [4], Smith, Dodia and Bowles [5]) focussed on experimental, theoretical and computational aspects of spots in boundary layers and allied flows. This was mostly for turbulent spots but also for laminar or transitional ones, which are more our concern here. Spots, which are three-dimensional unsteady patches of disturbed fluid progressing in otherwise undis-turbed motion, are important in technological as well as engineering and scien-tific terms [6] and their properties are reviewed broadly by [1-5] in particular. The three basic types are laminar, transitional and turbulent spots, depending on the amplitude and spectra of the initial disturbance, and all three are of much interest in terms of fundamental fluid dynamics and applications. A knowledge of spots is used in industrial research at Rolls Royce for example to model transition to turbulence, giving an estimate for the intermittency

factor. Numerous aspects of turbulent spots have been studied experimentally, with fascinating and somewhat varied results, for example on the main arrowhead-shaped part of the spots, its tail, its notional speed, and its spreading rate. Contributions stretch from Emmons [7], Schubauer and Klebanoff [8], Lighthill [9], Schlichting [10], Falco [11] to Head and Bandyopadhyay [12], Perry et al. [13], Chambers and Thomas [14], Smith et al. [15], Gad-el-Hak et al, [16], Katz et al. [17], Johansson et al. [18], Henningson and Alfredson [19] and Robinson [20]. Outstanding features found experimentally include the following. Much of the dynamics in a spot closely resembles that in a fully turbulent boundary layer; a turbulent spot develops fast, typically from localized disturbances with large initial amplitude; the subsequent growth and spreading of a fully turbulent spot probably take place in a domino-like manner, possibly associated with the successive production of hairpin vortices in the flow near the solid surface; the spanwise growth of the spot greatly exceeds the growth normal to the surface; and the leading edge and the spanwise side edges are notably sharp, with interaction between the spot and trailing wave packets especially near the sides. Again, a spot may be generated very rapidly (Elder [21]), even at subcritical Reynolds numbers, by a sufficiently strong initial disturbance bypassing the well-known natural routes through transition. Several other experimental features are also described in the above papers. Along with this, interesting direct numerical simulations have been performed on transitional/turbulent spots, mostly for channel flows and more recently for boundary layers. Most are confined to spatially periodic boundary conditions but, for a large period, they seem to reproduce fairly well some of the major experimental findings. Examples are in Leonard [22], Bullister and Orszag [23], Henningson et al. [24], Henningson and Kim [25], Lundbladh and Johansson [26], Fasel [27], Konzelmann and Fasel [28]. Much extra physical insight and understanding have still to be provided, nevertheless. Systematic tracking of the effects of increasing amplitude, for instance, largely remains to be done, both experimentally and computationally. Few, if any, systematic theoretical studies had been made either, until recently, especially on the scales and flow structures necessary for a clear physical understanding of the spot's behaviour. A strongly nonlinear theory is desirable, and the research below appears to be the only effort in that direction, specifically for spot evolution, i.e., the initial-value problem. Our approach here, combined with the related works [5], [29], [30], is to apply recent nonlinear theory and scaling arguments to address the experimental findings above. Much of these findings can be described by the theory, even though many complex phenomena arise during spot evolution.

  The present work aims at increased theoretical understanding of nonlinear spots in boundary layers based on the series [5, 6, 29–31] (see also [31] for jet flows and channel flows). Our concern is therefore more with transitional spots than with turbulent ones, the latter involving severe limitations in modelling even though most experiments are on the turbulent case. A survey of the theoretical spot structure is given in [5, 6], following the many earlier experimental studies of spots, e.g., in [1–5]. The latter as indicated above tend to establish the following main spot features: the characteristic arrowhead shape with overhanging leading edge, the calm region trailing behind, with accompanying edge disturbances, the spreading rates and speeds of the typical spot,

its maximum normal dimension being along its centre-line but the maximum turbulent intensity being at the edges.

The challenge and goal for the theory is to predict, post-dict, explain and understand all those main features. Some have been covered already in [5], [6] for instance. A significant part of the theory in [5], however, assumed or guessed certain nonlinear behaviour near the spot trailing edge without testing the important amplitude-dependent trends involved; an issue not settled in [5] or [6] is whether and how increased nonlinear dynamics from larger typical spot disturbance amplitudes, at increasing distances downstream, forces stronger disturbances towards the spot centre, in particular completing the description and prediction of the trailing edge of the spot. Here we test those important nonlinear trends, as described in more detail in the next paragraph. The corresponding theoretical spot structure is of necessity nonlinear and largely inviscid (of Euler type, see below) although there are undoubtedly significant connections with smaller-scale viscous properties including sublayer bursting as reviewed in [32], while [6] suggests that shortened-scale inviscid effects as well as nonlinearity help to fix the planform spreading angle of the spot at approximately $11°$, in line with experiments.

The first impact of nonlinearity as the representative disturbance amplitude increases downstream within the spot is felt mostly near the spot edges or wing-tips, according to analysis [5, 30] and to the experiments above. Here as in the last two references we address the three-dimensional flow response at the spot trailing edge initially but at amplitudes increased from those studied in detail previously. Keeping track of the influences of increasing amplitudes is clearly important both theoretically and physically, as above, and it needs a concerted effort as pointed out in [5]. As anticipated in the preceding paragraph for example there is the critical issue of whether and precisely how nonlinear effects feed inwards, from their first impact at the wing-tips, to produce second impacts and so on which eventually affect the entire centre of the trailing-edge zone and thence the main body of the spot (the mid-spot), as suggested in [5]. See Fig. 1. These influences of enhanced amplitude are associated with the two main zones of the globally inviscid spot emerging at large scaled times t [5, 6, 29–32], the trailing zone containing the calmed region [6] and the mid-spot zone, respectively at scaled distances of order $t^{1/2}$ and t downstream of the spot initiation position. Within those zones and in-between nonlinear responses arise first in the form of interactions between the (relatively slow) mean flow part and the (relatively fast) fluctuations or waves present, dominated by interplay between a first harmonic and corresponding mean-flow corrections, with second harmonics and so on remaining negligible. These initially involve pressure-displacement balances [5, 6, 30–32] between the boundary layers and the free stream outside, unlike the interactions in [33], although in fact those balances are found in the current study to become secondary as the typical amplitudes continue to increase. For new mean-flow momentum contributions then come into play, additional to those in [30], and these lead to substantial changes in the nature of the wave/mean-flow non-linear interactions. In particular strong effects turn out to be provoked by enhanced variations in phase at such higher amplitudes.

The first part of this work, in Sections 2–5, is devoted to the so-called level II of amplitudes [5], corresponding to the second impacts described in the
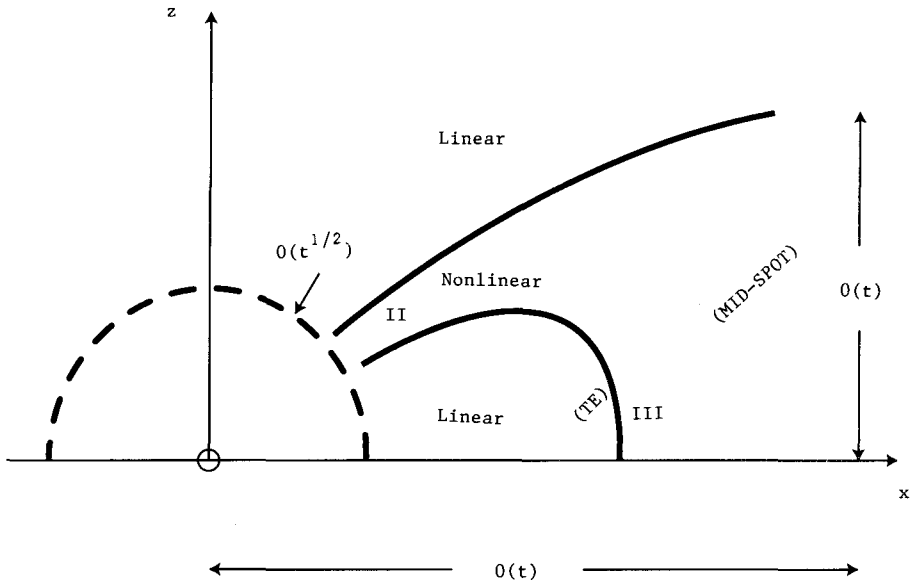
Figure 1. Sketch of the flow structure, for level II (see Sections 2–5) and for higher amplitudes (Sections 6, 7) up to level III, showing nonlinearity gradually feeding in from the wing-tips to the centre of the trailing edge (TE) region.

previous paragraph as opposed to the level I of smaller amplitudes in [30]. The trailing-edge zone is set up in Section 2, followed by analysis of increasing amplitudes concentrated in wing-tip regions just downstream in Sections 3, 4 including the role of a thin wall layer. The resulting interaction equations are studied in Section 5. The main new physical feature here is the enhanced role of the mean-flow inertial effects in fixing the flow response.

Then the second part, in Section 6, addresses amplitudes increased still further, just above those of level II. The details of the working in the first part in fact enable this second part to be dealt with by adjustments of that working, incorporating especially the new phase variations which become more and more powerful physically. A sequence of such amplitude increases downstream eventually forces the nonlinear wing-tip layer(s) to expand and spread inwards to cover the whole trailing-edge zone as amplitude level III is encountered [5, 30], in a strongly nonlinear manner. This sequence involving the near-wall momentum and Reynolds stresses acting in concert bridges the gap in detail left by [5], confirming the trend of the theoretical trailing-edge response as well as the spot centre supposed in that paper and drawn in Fig. 1 above. The repercussions at higher amplitudes are considered briefly in Sections 6, 7, along with final comments in Section 7. The build-up process nonlinearly inward from the wing-tips, in "echelon" style as described in Section 6, *cf.* the domino process earlier, provides an explanation of the trailing-edge behaviour as well as the calm, linear, zone behind it, an explanation which apparently no other theory has been able to provide.

The major context of concern here is that governed by the three-dimensional unsteady Euler equations, holding locally throughout the incompressible

boundary layer,

$$\mathbf{\nabla}\cdot\mathbf{u}=0, \tag{1.1a}$$

$$(\partial_t+\mathbf{u}\cdot\mathbf{\nabla})\mathbf{u}=-\mathbf{\nabla}p, \tag{1.1b}$$

where $\mathbf{u}=(u, v, w)$ and the associated Cartesian coordinates x, y, z (streamwise, normal, spanwise, in turn) are scaled with respect to the local free-stream speed and typical boundary-layer thickness $O(\mathrm{Re}^{-1/2})$ respectively. The global Reynolds number Re is large. The time t and pressure p are likewise based on $O(\mathrm{Re}^{-1/2})$, $O(1)$ scales in turn, while $\mathbf{\nabla}$ denotes $(\partial_x, \partial_y, \partial_z)$. The boundary conditions include

$$[\mathbf{u}, p]\to\begin{cases}[1, 0, 0, 0] & \text{as } y\to\infty,\\ [u_B(y), 0, 0, 0] & \text{as } x^2+z^2\to\infty,\end{cases} \tag{1.1c, d}$$

$$v=0 \quad\text{at}\quad y=0, \tag{1.1e}$$

$$[\mathbf{u}, p] \quad\text{prescribed at}\quad t=0, \tag{1.1f}$$

cf the generalization in [5]. The original velocity profile $u_B(y)$ is monotonic (*e.g.*, Blasius) with $u_B(\infty)=1$ and the scaled skin friction $u_B'(0)$ is normalized to be unity. All the subsequent work in the paper stems from (1.1a–f). This is for the global, inviscid, structure of the typical spot, whereas more localized viscous effects, eruptions, and their interactions with the global structure, are discussed in [32]. The Euler stage of (1.1a–f) corresponds to nonlinear disturbance wavenumbers α, β, frequencies ω, propagation speeds c and amplitudes (for example, pressure p', velocity u') all of $O(1)$, based on the boundary-layer thickness and local freestream speed, thus representing a wider range than conventional linear-type TS disturbances, which have $\alpha, \beta, \omega, c, |p'|, |u'|$ all smaller by an order of magnitude. In consequence, it seems not unreasonable to tackle the free spot-evolution problem theoretically first by means of the Euler-stage approach, but as a nonlinear three-dimensional initial-value problem for a localized input disturbance. This is the concern of the following sections.

§2. *The spot trailing-edge.* Our interest here is in gaining extra insight into the flow features at the so-called trailing edge of the spot. To that end we examine the downstream $O(t^{1/2})$ zone, for large times t, as spatially it lags behind the mid-spot $O(t)$ zone further downstream, but we then move on to tackle the region between the two by considering increased distances downstream, corresponding to increasing typical amplitudes.

So we start by addressing the zone where $(X, Z)\equiv t^{-1/2}(x, z)$ are of order unity. There the solution of the Euler equations (1.1) takes on a three-tiered structure [30] in the y direction, the inner tier having $y=t^{-1/2}Y$ with $Y\sim 1$, well inside the boundary layer, and producing the thin-layer system

$$U_X+V_Y+W_Z=0, \tag{2.1a}$$

$$-\tfrac{1}{2}U+(U-\tfrac{1}{2}X)U_X+(V+\tfrac{1}{2}Y)U_Y+(W-\tfrac{1}{2}Z)U_Z=-P_X, \tag{2.1b}$$

$$-\tfrac{1}{2}W+(U-\tfrac{1}{2}X)W_X+(V+\tfrac{1}{2}Y)W_Y+(W-\tfrac{1}{2}Z)W_Z=-P_Z. \tag{2.1c}$$

Here $(u, w) \sim t^{-1/2}(U, W)$, $v \sim t^{-3/2}V$, $p \sim t^{-1}P$, where $P(X, Z)$ is independent of Y, and the boundary conditions are

$$V = 0 \quad \text{at} \quad Y = 0, \tag{2.1d}$$

$$U \sim Y + A(X, Z), \quad W \to 0, \quad \text{as} \quad Y \to \infty, \tag{2.1e}$$

for tangential flow at the solid surface and for matching with the middle tier wherein $y \sim 1$. The unknown pressure P and negative displacement A are linked *via* the quasi-potential flow properties in the outer tier, outside the boundary layer, where $y \sim t^{1/2}\bar{y}$ say, $p \sim t^{-1}\bar{p}$, and $\bar{p}(X, \bar{y}, Z)$ must satisfy

$$(\partial_X^2 + \partial_{\bar{y}}^2 + \partial_Z^2)\bar{p} = 0 \tag{2.2a}$$

subject to

$$\bar{p} \quad \text{bounded} \quad \text{in} \quad \text{the} \quad \text{farfield}, \tag{2.2b}$$

$$\bar{p} \to P, \quad \bar{p}_{\bar{y}} \to A_{XX}, \quad \text{as} \quad \bar{y} \to 0+. \tag{2.2c}$$

The constraint (2.2c) matches the outer- and middle-tier solutions. In general the response in the $O(t^{1/2})$ zone is controlled by (2.1a)–(2.2c).

Relatively large distances are to be taken next, so that X, Z are large and positive. This forms the basis of the study in the succeeding sections. Earlier [29] considered linear disturbances, followed by [5, 30] who investigated among other features a first nonlinear stage (level I) arising in an edge layer near the wing-tip $Z = \mu X$, where the constant $\mu = 8^{-1/2}$. The present study is aimed at amplitudes slightly increased above those in the last two references, and the orders of magnitude involved in the scalings and expansions below may be inferred from the solution properties in those references. What is new about the present stage (level II) is, mainly, a significant contribution from the inertial effects of the mean flow correction.

§3. *The response inside the boundary layer.* Guided by the remarks in Section 2 on lower amplitudes, the new solution of concern here, for the inner equations, expands in the form

$$U = Xs + X^{-1/4}(Eu_{01} + c.c.) + X^{-1/2}u_{00} + X^{-3/4}(Eu_{11} + c.c.)$$

$$+ \ldots + X^{-5/4}(Eu_{21} + c.c.)$$

$$+ X^{-3/2}(E^2 u_{22} + c.c.) + X^{-7/4}(Eu_{31} + c.c.) + \ldots, \tag{3.1a}$$

$$V = X^{7/4}(Ev_{01} + c.c.) + X^{5/4}(Ev_{11} + c.c.)$$

$$+ X^{3/4}(Ev_{21} + c.c.) + X^{1/2}v_{20} + \ldots, \tag{3.1b}$$

$$W = X^{-1/4}(Ew_{01} + c.c.) + X^{-1/2}w_{00} + X^{-3/4}(Ew_{11} + c.c.) + \ldots, \tag{3.1c}$$

for large X, together with the pressure and displacement expansions

$$P = X^{3/4}(Eg_{01} + c.c.) + X^{1/4}(Eg_{11} + c.c.)$$

$$+ X^{-1/4}(Eg_{21} + c.c.) + X^{-1/2}g_{20} + \ldots, \tag{3.1d}$$

$$A = X^{-1/4}(EA_{01} + c.c.) + X^{-1/2}A_{00} + X^{-3/4}(EA_{11} + c.c.) + \dots \quad (3.1e)$$

Here $s \equiv X^{-1}Y$, $\bar{\eta} \equiv Z - \mu X$ are both of $O(1)$, c.c. denotes the complex conjugate and the wave contribution is

$$E \equiv \exp\left[i(b_1 X^2 + \lambda X \bar{\eta} + X^{1/2}f(\bar{\eta}))\right], \quad (3.2)$$

with the constants b_1, λ and the phase function f to be determined. The possibility of three values for f is mentioned later in Section 5. Again, $u_{01}, u_{11}, u_{21}, u_{22}$, etc., denote wave parts involved with powers of E while u_{00}, v_{20}, w_{00} are mean-flow parts. In the following we have to proceed to several orders in the E-terms to derive the major results.

Substitution of (3.1a–e) into the governing equations (2.1) yields, at first order, the system

$$(\mathscr{L}, \mathscr{M}, \mathscr{N})(\mathbf{u}_{01}) = 0 \quad (3.3a)$$

controlling the main E-components. Here the operators (of continuity and momentum) are defined by

$$\mathscr{L}(\mathbf{u}) \equiv iBu + v_s + \lambda iw, \quad (3.3b)$$

$$\mathscr{M}(\mathbf{u}) \equiv (s - \tfrac{1}{2})iBu + v - \tfrac{1}{2}\mu\lambda iu + iBg, \quad (3.3c)$$

$$\mathscr{N}(\mathbf{u}) \equiv (s - \tfrac{1}{2})iBw - \tfrac{1}{2}\mu\lambda iw + i\lambda g, \quad (3.3d)$$

respectively, while $\mathbf{u}$ now stands for (u, v, w, g) and the constant $B \equiv (2b_1 - \lambda\mu)$. Hence the dominant solution form, satisfying the boundary conditions at the wall and at large Y, is given by

$$u_{01} = A_{01} + \lambda^2 g_{01}B^{-1}\delta^{-1}, \quad v_{01} = -iBA_{01}s, \quad w_{01} = -\lambda g_{01}\delta^{-1}, \quad (3.4a\text{–}c)$$

with

$$q_{01} = BA_{01}, \quad Bb_1A_{01} = \beta^2 g_{01}, \quad \delta \equiv Bs - b_1, \quad \beta \equiv (B^2 + \lambda^2)^{1/2}, \quad (3.4d\text{–}g)$$

and we set the skew velocity $q \equiv Bu + \lambda w$ for convenience. We should comment that here and below there is a passive nonlinear critical layer at $\delta = 0$ and a wall layer at $s = 0+$ which is addressed later. The amplitude function $g_{01}(\bar{\eta})$ remains unknown at this level.

At second order, the continuity and momentum balances become

$$\mathscr{L}(\mathbf{u}_{11}) - \mu if'u_{01} + if'w_{01} = 0, \quad (3.5a)$$

$$\mathscr{M}(\mathbf{u}_{11}) - s\mu if'u_{01} = \mu if'g_{01}, \quad (3.5b)$$

$$\mathscr{N}(\mathbf{u}_{11}) - s\mu if'w_{01} = -if'g_{01}, \quad (3.5c)$$

the extra terms being due to the phase contribution f in (3.2). Here the prime denotes differentiation with respect to $\bar{\eta}$. The solution therefore gives

$$u_{11} = A_{11} + 2b_1 f'\lambda^2 g_{01}B^{-2}\delta^{-1} + \mu f's\lambda^2 g_{01}B^{-1}\delta^{-2}$$
$$+ \lambda(\lambda g_{11} + f'g_{01})B^{-1}\delta^{-1}, \quad (3.6a)$$

$$w_{11} = -\mu f's\lambda g_{01}\delta^{-2} - (\lambda g_{11} + f'g_{01})\delta^{-1}, \quad (3.6b)$$

$$q_{11} = BA_{11} + 2b_1 f'\lambda g_{01}B^{-1}\delta^{-1}, \quad (3.6c)$$

with

$$b_1\{BA_{11} - 2f'\lambda g_{01}B^{-1}\} = \beta^2 g_{11} - f'(\mu B - \lambda)g_{01},\tag{3.6d}$$

in view of the boundary conditions at small and large Y.

Similar working applies at higher orders. Thus the *third order* equations for the E-terms are

$$\mathcal{L}(\mathbf{u}_{21}) - \mu i f' u_{11} + \lambda \bar{\eta} i u_{01} - \mu u_{01\bar{\eta}} + i f' w_{11} + w_{01\bar{\eta}} = 0,\tag{3.7a}$$

$$\mathcal{M}(\mathbf{u}_{21}) - s\mu i f' u_{11} + (s-1)\lambda \bar{\eta} i u_{01} - s\mu u_{01\bar{\eta}}$$

$$= \mu i f' g_{11} - \lambda \bar{\eta} i g_{01} + \mu g'_{01},\tag{3.7b}$$

$$\mathcal{N}(\mathbf{u}_{21}) - s\mu i f' w_{11} + (s-1)\lambda \bar{\eta} i w_{01} - s\mu w_{01\bar{\eta}}$$

$$= -i f' g_{11} - g'_{01},\tag{3.7c}$$

showing the first appearance of $\bar{\eta}$ derivatives, among other effects, while the *fourth order E* balances give

$$\mathcal{L}(\mathbf{u}_{31}) - \mu i f' u_{21} + \lambda \bar{\eta} i u_{11} - \mu u_{11\bar{\eta}} + \tfrac{1}{2} i f u_{01} + i f' w_{21} + w_{11\bar{\eta}} = 0,$$

$$\mathcal{M}(\mathbf{u}_{31}) - s\mu i f' u_{21} + (s-1)\lambda \bar{\eta} i u_{11} - s\mu u_{11\bar{\eta}} + \tfrac{1}{2}(s-\tfrac{1}{2})i f u_{01} - \tfrac{1}{2}\bar{\eta} i f' u_{01} + A_{00} B i u_{01}\tag{3.8a}$$

$$= \mu i f' g_{21} - \lambda \bar{\eta} i g_{11} + \mu g'_{11} - \tfrac{1}{2} i f g_{01},$$

$$\mathcal{N}(\mathbf{u}_{31}) - s\mu i f' w_{21} + (s-1)\lambda \bar{\eta} i w_{11} - s\mu w_{11\bar{\eta}} + \tfrac{1}{2}(s-\tfrac{1}{2})i f w_{01}\tag{3.8b}$$

$$- \tfrac{1}{2}\bar{\eta} i f' w_0 + A_{00} B i w_{01} = -i f' g_{21} - g'_{11},\tag{3.8c}$$

showing further linear influences but also the first nonlinear effects, proportional to A_{00} in (3.8b, c). Here the solution for the mean-flow correction, given in (3.11a–c) below, has been inserted in (3.8b, c). Solving (3.7a–c), then, with the displacement condition at large s and the tangential-flow constraint as $s \to 0$, we obtain

$$iBq_{21} = 4b_1 i\mu f'^2 B^{-1}\lambda g_{01}(\tfrac{1}{2}b_1\delta^{-2} + \delta^{-1}) + iB^2 A_{21}$$

$$+ \delta^{-1}\{2b_1 i f'(\lambda g_{11} + f' g_{01}) + 2b_1\lambda g'_{01} - \lambda^3 i\bar{\eta} g_{01}\}\tag{3.9a}$$

for the skewed velocity component, with

$$-b_1 B^{-1}[iB^2 A_{21} - 2\mu i f'^2 \lambda g_{01} B^{-1} - 2i f'(\lambda g_{11} + f' g_{01}) - 2\lambda g'_{01} + \lambda^3 i\bar{\eta} b_1^{-1} g_{01}]$$

$$= i\lambda \bar{\eta} B A_{01} - i\beta^2 g_{21} + (\mu B - \lambda)(i f' g_{11} + g'_{01}) - B\lambda \bar{\eta} i g_{01}.\tag{3.9b}$$

Likewise, the skewed component q_{31} can be evaluated from (3.8b–c), leading to the relation

$$\{\tfrac{1}{4}(B + 2b_1)f + (\tfrac{1}{2}B - \lambda\mu)\bar{\eta} f' - B^2 A_{00}\}A_{01} + \lambda(B + b_1)\bar{\eta} A_{11}$$

$$+ \mu i b_1 A'_{11} - b_1\mu f' A_{21} + b_1 B A_{31}$$

$$= \beta^2 g_{31} + 2(\lambda - \mu B)f' g_{21}$$

$$+ \{2B\lambda\bar{\eta} + (\mu^2 + 1)f'^2\}g_{11} + 2(\mu B - \lambda)i g'_{11}$$

$$+ \{Bf - 2\lambda\mu\bar{\eta} f' - i(\mu^2 + 1)f''\}g_{01} - 2(\mu^2 + 1)i f' g'_{01}\tag{3.10}$$

involving A_{31}, g_{31}, higher derivatives of the unknown phase function f, and the main nonlinear effect so far, due to A_{00}. The results (3.4e), (3.6d), (3.9b),

(3.10) serve as internal relations between A_{n1}, g_{n1} ($n = 0, 1, 2, 3$) which are to be combined with the external relations found in Section 4 below.

The *mean flow effects* need to be described next, and these arise mainly at two levels, as far as the inside of the boundary layer is concerned. The first is in the controlling equations for (u_{00}, v_{20}, w_{00}) derived from the dominant E^0 contributions. The amplitude-squared forcings due to the wave-inertial terms at this level are

$$(v_{01} \partial u_{01}^* / \partial s - \lambda i w_{01} u_{01}^* + c.c.), \qquad (-Bi u_{01} w_{01}^* + v_{01} \partial w_{01}^* / \partial s + c.c.)$$

in the X, Z momentum equations respectively [* denotes *c.c.*], at the order $X^{1/2} E^0$, but these forcings work out to be identically zero in view of the solutions (3.4a–c). Hence we find, using equations similar to (3.12a–c) below, that

$$u_{00} = A_{00}, \quad v_{20} = \mu s A_{00}', \quad w_{00} = 0, \qquad (3.11a\text{--}c)$$

results which were anticipated in (3.8b, c). The reason for $A_{00}(\bar{\eta})$ being nonzero will become apparent in Section 4. Similar cancellation in the momentum equations occurs at $O(1)$. The next level then leads to the controlling equations for (u_{20}, v_{40}, w_{20}), the mean-flow contributions of orders $X^{-3/2}, X^{-1/2}, X^{-3/2}$ respectively in (3.1a–c), namely

$$-\mu u_{20\bar{\eta}} - \tfrac{1}{2} A_{00} + v_{40s} + w_{20\bar{\eta}} = 0, \qquad (3.12a)$$

$$-s\mu u_{20\bar{\eta}} + v_{40} + F_1 = \mu g_{20}', \qquad (3.12b)$$

$$-s\mu w_{20\bar{\eta}} + F_2 = -g_{20}', \qquad (3.12c)$$

where, on use of (3.11a–c), the forcing terms present are

$$F_1 = -\tfrac{1}{2} A_{00}(s + \tfrac{1}{2}) - \tfrac{1}{2} \bar{\eta} A_{00}'$$

$$+ [-\mu u_{01} u_{01\bar{\eta}}^* + v_{21} u_{01s}^* + v_{11} u_{11s}^* + v_{01} u_{21s}^* + w_{01}(-\lambda i u_{21}^* - i f' u_{11}^* + u_{01\bar{\eta}}^*)$$

$$+ w_{11}(-\lambda i u_{11}^* - i f' u_{01}^*) - w_{21} i \lambda u_{01}^*] + c.c., \qquad (3.12d)$$

$$F_2 = [u_{01}(-iB w_{21}^* + \mu i f' w_{11}^* - \lambda \eta i w_{01}^* - \mu w_{01\bar{\eta}}^*)$$

$$+ u_{11}(-iB w_{11}^* + \mu i f' w_{01}^*) - u_{21} iB w_{01}^*$$

$$+ v_{21} w_{01s}^* + v_{11} w_{11s}^* + v_{01} w_{21s}^* + w_{01} w_{01\bar{\eta}}^*] + cc., \qquad (3.12e)$$

and include both wave-amplitude-squared effects and mean-displacement effects.

A relation between the mean pressure g_{20}, the mean displacement $-A_{00}$ and the wave amplitude g_{01} then follows from examining the behaviour of (3.12a–e) as $s \to 0+$, combined with the flow response in a relatively thin wall layer that lies between the present $s \sim 1$ zone and the surface. This is a somewhat delicate matter, as (3.12b, c) appear at first sight to lead to different results. The resolution is provided by the wall-layer solution, which is similar to the ones examined by Smith [30], Dodia [31] and suggests that, as $s \to 0+$, v_{40} tends to zero but u_{20}, w_{20} become unbounded like s^{-1}. Hence we obtain the relation

$$g_{20}' = -\beta^2 b_1^{-2} (|g_{01}|^2)' - \tfrac{1}{2} \mu (\mu^2 + 1)^{-1} (\tfrac{1}{2} A_{00} + \bar{\eta} A_{00}') \qquad (3.13)$$

linking g_{20}, A_{00}, g_{01}. The three other equations required to determine these three unknown functions and the phase term f, all of which are coupled together, are obtained in the next section.

The final balance required from the properties in the present zone comes from the *fifth order* terms in E. Their governing equations follow the pattern of (3.3a), (3.5), (3.7), (3.8), *i.e.*, forcings of $(\mathscr{L}, \mathscr{M}, \mathscr{N})(\mathbf{u}_{41})$, and likewise for their solutions, which are quite complicated. Again omitting the detailed working, we find that the internal relation at this level is

$$b_1 B A_{41} - \mu b_1 f' A_{31} + (B + b_1)\lambda\bar{\eta}A_{21} + \mu i b_1 A'_{21}$$

$$+ \{\tfrac{1}{4}(B + 2b_1)f - (\lambda\mu - \tfrac{1}{2}B)\bar{\eta}f' - B^2 A_{00}\}A_{11}$$

$$+ \{-\tfrac{1}{4}\mu ff' - \tfrac{1}{2}\mu\bar{\eta}f'^2 + \lambda^2\bar{\eta}^2 + i(\tfrac{1}{2}b_1 - \tfrac{3}{8}B) - B^2 A_{10} + 2\mu Bf' A_{00}\}A_{01}$$

$$+ i(\mu\lambda - \tfrac{1}{2}B)\bar{\eta}A'_{01}$$

$$= \beta^2 g_{41} + 2(\lambda - \mu B)(f'g_{31} - ig'_{21})$$

$$+ \{2B\lambda\bar{\eta} + (\mu^2 + 1)f'^2\}g_{21} - 2if'(\mu^2 + 1)g'_{11}$$

$$+ \{Bf - 2\lambda\mu\bar{\eta}f' - i(\mu^2 + 1)f''\}g_{11}$$

$$+ \{-\tfrac{5}{2}Bi - \mu ff' + \lambda^2\bar{\eta}^2 + i\lambda\mu\}g_{01} + 2i\lambda\mu\bar{\eta}g'_{01} - (\mu^2 + 1)g''_{01}, \qquad (3.14)$$

connecting A_{41}, g_{41}, further contributions from the phase f, and the primary and secondary mean-flow-correction effects A_{00}, A_{10}.

§4. *Outside the boundary layer.*   The external relations between the g's and A's all stem from (2.2a–c), holding outside the boundary layer, coupled with an expansion for $\bar{p}$ analogous with that in (3.1d). Thus at leading order $\bar{g}_{01}$ satisfies $(\partial^2/\partial\bar{y}^2 - \beta^2)\bar{g}_{01} = 0$, subject to

$$\bar{g}_{01} \to g_{01}, \quad \partial\bar{g}_{01}/\partial\bar{y} \to B^2 A_{01} \quad \text{as} \quad \bar{y} \to 0+, \quad \bar{g}_{01} \to 0 \quad \text{as} \quad \bar{y} \to \infty,$$

where $\bar{y} = X^{-1}\bar{y}$. So

$$\bar{g}_{01} = g_{01}\exp(-\beta\bar{y}), \quad \text{and} \quad \beta g_{01} = B^2 A_{01} \qquad (4.1)$$

provides the first external relation.

Pursuing the same pattern to higher order we then obtain after some working the second-to-fifth external relations for the E terms,

$$\beta g_{11} = B^2 A_{11} - 2\mu Bf' A_{01} - f'\beta^{-1}(\lambda - \mu B)g_{01}, \qquad (4.2)$$

$$\beta g_{21} = B^2 A_{21} - 2\mu Bf' A_{11} + (2B\lambda\bar{\eta} + \mu^2 f'^2)A_{01} + 2\mu iBA'_{01} + \sigma_2, \qquad (4.3)$$

$$\beta g_{31} = B^2 A_{31} - 2\mu Bf' A_{21} + (2B\lambda\bar{\eta} + \mu^2 f'^2)A_{11} + 2\mu iBA'_{11}$$

$$+ (Bf - 2\lambda\mu\bar{\eta}f' - \mu^2 if'')A_{01} - 2\mu^2 if' A'_{01} + \sigma_3, \qquad (4.4)$$

$$\beta g_{41} = B^2 A_{41} - 2\mu Bf' A_{31} + (2B\lambda\bar{\eta} + \mu^2 f'^2)A_{21} + 2\mu iBA'_{21}$$

$$+ (Bf - 2\lambda\mu\bar{\eta}f' - \mu^2 if'')A_{11} - 2\mu^2 if' A'_{11}$$

$$+ (\lambda^2\bar{\eta}^2 - \mu ff' + i\lambda\mu - \tfrac{1}{2}iB)A_{01} + 2\lambda\mu i\bar{\eta}A'_{01} - \mu^2 A''_{01} + \sigma_4, \quad (4.5)$$

in turn. Here the σ_n, $n = 2, 3, 4$, are defined in Appendix A. The mean-flow contribution in contrast has $\bar{y}$ remaining of order unity and leads to the relation

$$g_{20} = \pi^{-1}(\mu^2 + 1)^{-1/2}\mu^2 \ \overline{\int_{-\infty}^{\infty}} \ A_{00}'(\xi)(\bar{\eta} - \xi)^{-1}d\xi \qquad (4.6)$$

between g_{20}, A_{00}, from (2.2a–c), with the bar in the integral sign denoting the Cauchy principal value.

In the next section the external relations (4.1)–(4.6) are coupled with the corresponding internal relations, (3.4e), (3.6b), (3.9d), (3.10), (3.14), (3.13), respectively, to yield the nonlinear controlling equations for the wave amplitude g_{01}, the phase f and the mean-flow part A_{00}.

§5. *The interaction equations and solution properties.* When the internal and external pressure-displacement relations of the previous two sections are combined, the first three levels of working for the E terms act to confirm the self-consistency of the values of the constants,

$$b_1 = \frac{3^{3/2}}{16}, \quad B = \frac{3^{1/2}}{4}, \quad \lambda = \left(\frac{3}{8}\right)^{1/2}, \quad \mu = 8^{-1/2}, \quad \beta = \frac{3}{4}, \qquad (5.1)$$

as in previous papers. The fourth level however, *i.e.*, taking (3.10) with (4.4), is found to yield the balance

$$2^{1/2}f'^3 + 2\bar{\eta}f' - f = (4/3^{1/2})\beta A_{00}, \qquad (5.2)$$

between the phase and the mean part. Then the fifth-level contributions (3.14), (4.5) in E lead to a lengthy complex equation for $g_{01}(\bar{\eta})$, of which the real part eventually gives the equation

$$\left[\frac{1}{4} + \frac{3}{\sqrt{2}}f'f''\right]|g_{01}| + \left[\bar{\eta} + \frac{3}{\sqrt{2}}f'^2\right](|g_{01}|)' = 0, \qquad (5.3)$$

balancing phase and wave-amplitude effects. The system of interaction equations is then closed by coupling (3.13), (4.6) to obtain the balance

$$\frac{-\frac{1}{2}\mu}{(\mu^2 + 1)}(\tfrac{1}{2}A_{00} + \bar{\eta}A_{00}') - \frac{\beta^2}{b_1^2}(|g_{01}|^2)' = \frac{\mu^2}{\pi(\mu^2 + 1)^{1/2}} \int_{-\infty}^{\infty} \frac{A_{00}''(\xi)d\xi}{(\bar{\eta} - \xi)} \qquad (5.4)$$

between the wave-amplitude and the mean-flow parts.

The nonlinear interaction is therefore governed by the three equations (5.2)–(5.4) for the unknown functions f, A_{00}, $|g_{01}|$, over the range $-\infty < \bar{\eta} < \infty$. These require a numerical treatment, which was undertaken as described below. Concerning the earlier studies of [5], [30] for lower amplitudes, the trend towards their results occurs at relatively low amplitudes $|g_{01}|$, A_{00}, with the scale $|\bar{\eta}|$ then shrinking, such that $|g_{01}|$, A_{00}, f become of order $|\bar{\eta}|^m$, $m = \frac{1}{4}, \frac{3}{2}, \frac{3}{2}$ respectively. This has the effect of relegating the two A_{00} terms on the

left-hand side of (5.4) to higher order, in line with the work in the last study: again see below. At general amplitudes however those two terms remain, representing mean-flow inertial contributions distinct from those of the previous studies.

Computational solutions of (5.2)–(5.4) were sought in a normalized form obtained by setting

$$[f, \bar{\eta}, A_{00}, |g_{01}|] = [\hat{\sigma}_1 f_c, \hat{\sigma}_2 \eta_c, \hat{\sigma}_3 a_c, \hat{\sigma}_4 p_c]. \qquad (5.5a)$$

Here the constants $\hat{\sigma}_{1-4}$ satisfy

$$\hat{\sigma}_1 = \frac{\hat{\sigma}_2^{3/2}}{2^{1/4}}, \quad \hat{\sigma}_3 = \frac{2\beta^2(\mu^2+1)\hat{\sigma}_4^2}{b_1^2\hat{\sigma}_2\mu}, \quad \frac{\hat{\sigma}_2^{5/2}}{2^{1/4}} = \frac{8\beta^3(\mu^2+1)\hat{\sigma}_4^2}{3^{1/2}b_1^2\mu}, \qquad (5.5b)$$

fixing $\hat{\sigma}_{1-3}$, with $\hat{\sigma}_4 \equiv |g_{01}|(\bar{\eta}=0)$ acting as a given amplitude parameter such that $p_c(0)=1$. The governing equations thus become

$$h_c^3 + 2\eta_c h_c - f_c = a_c \quad (\text{where } h_c = f_c'), \qquad (5.6)$$

$$(\eta_c + a_2 h_c^2)p_c' + (\tfrac{1}{4} + a_2 h_c h_c')p_c = 0, \qquad (5.7)$$

$$-(\tfrac{1}{2}a_c + \eta_c a_c') - (p_c^2)' = \frac{1}{\Gamma_0\pi} \int_{-\infty}^{\infty} \frac{a_c''(q)dq}{(\eta_c - q)} \qquad (5.8)$$

where the parameter $\Gamma_0 \equiv \tfrac{1}{2}\hat{\sigma}_2^2\mu^{-1}(\mu^2+1)^{-1/2}$ increases with increasing amplitude $|g_{01}|(\bar{\eta}=0)$, while $a_2 = 3/2$. Cf. Section 4 of [5]. The iterative numerical procedure used is basically as follows, for a prescribed value of Γ_0. Given a latest guess for $F\{\equiv(p_c^2)'\}$, equation (5.8) is solved for a new $a_c(\eta_c)$ distribution, then (5.6) for f_c, h_c, then (5.7) for $p_c(\eta_c)$ subject to $p_c(0)=1$, and then $2p_c p_c'$ provides a revised guess for F, and so on, until convergence. Concerning more details of the finite-differencing within the above procedure, the solution of (5.6) was derived by Newtonian iteration with due attention to choosing the correct one of the three branches for h_c, f_c [9], while for (5.7) two-point marching was adopted. For the solution of (5.8) for a_c, we took a Fourier transform approach after some preliminary trials. This gives the transform ($\mathscr{F}$) of a_c as

$$\mathscr{F}(a_c) = \omega^{-1/2}e^{\pm i\omega^2/2\Gamma_0}\left\{ \int_0^\omega \mathscr{F}(F)\hat{\omega}^{-1/2}e^{\mp i\hat{\omega}^2/2\Gamma_0}d\hat{\omega} + \hat{B} \right\} \qquad (5.9)$$

when the transform variable ω is real and positive/negative respectively. Careful inversion of (5.9) combining analysis and numerical means therefore yields the updated a_c numerically. The value of $\hat{B}$ is chosen to avoid unacceptable wavelike behaviour locally. Both the computations and an analysis for small Γ_0 imply that $\hat{B}$ is nonzero in general. Computational results are presented in

Figs. 2, 3 for a representative value of Γ_0, other results obtained being very similar to these.

It is of interest that imposing small values of Γ_0 takes the solution back to level I in essence [5], [30]. The main scales involved then have $h_c, f_c, \eta_c, a_c, p_c$ of the respective orders $\Gamma_0, \Gamma_0^3, \Gamma_0^2, \Gamma_0^3, 1$. That leaves, in (5.8), the new terms $\frac{1}{2}a_c + \eta_c a_c'$ being negligible by a relative amount of order Γ_0^5, matching with the level-I balances as required. There is in addition however an outer region where those new terms reassert themselves, with η_c large and $O(\Gamma_0^{-1/2})$. In contrast, at relatively high amplitudes where Γ_0 becomes large, the integral contribution in (5.8) becomes secondary, since all the variables $h_c, f_c, \eta_c, a_c, p_c$ then simply remain of $O(1)$. Numerical solutions in this limit of large Γ_0, which are shown in Fig. 4, were derived from applying a fourth-order Runge–Kutta shooting scheme to (5.8) without the integral term.

The large-Γ_0 limit above shows a diminishing of the mean-flow influence produced by the flow near the external stream, such that the main balance left is between near-wall effects alone, namely those of the mean-flow momentum and of the Reynolds stresses due to the amplitude-squared inertia from the dominant fluctuations. Our next step is to consider the new stage or stages that must arise as the amplitude level continues to increase. Eventually we would expect the whole of the trailing edge to be affected nonlinearly as in [5] but prior to that important adjustments take place at amplitudes (and thickness scales) slightly above those in the current level II. These adjustments are considered in the next section.

§6. *Increased disturbance amplitudes.* As the amplitude of the disturbance is increased further, the effects of nonlinearity are felt across progressively wider edge layers, astride the $O(1)$ edge layer described in the first part of this work. The flow in these layers may be studied in an analogous fashion. The interaction equations given in Section 5 are shown below to be a particular system in a set of such systems of equations, each valid for a particular amplitude level and corresponding edge layer.

We define the edge-layer variable η now by $Z - \mu X = \eta X^n$. Thus the previous $O(1)$ edge layer is the case where $n = 0$ [level II]. At the other extreme, if $n = 1$ [level III], then the region of significant nonlinear effects extends across the entire trailing edge and can no longer be treated as an edge layer. See Fig. 1. We therefore constrain n by the condition $0 < n < 1$. Order-of-magnitude arguments indicate that the first new edge layer occurs when $n = 1/5$. An infinite set of values for n is in fact generated, each corresponding to a new layer, as we see below.

The expansions for the flow variables may be found in terms of n as

$$U = Xs + X^{(-1+5n)/4}(Eu_0 + c.c.) + X^{(-1+3n)/2}u_m + X^{(-3+7n)/4}(Eu_{11} + c.c.)$$

$$+ X^{(-5+9n)/4}(Eu_{21} + c.c.) + X^{(-6+10n)/4}(E^2u_{22} + c.c.)$$

$$+ X^{(-7+11n)/4}(Eu_{31} + c.c.) + \ldots + X^{(-3+5n)/2}u_{2m} + \ldots, \qquad (6.1a)$$
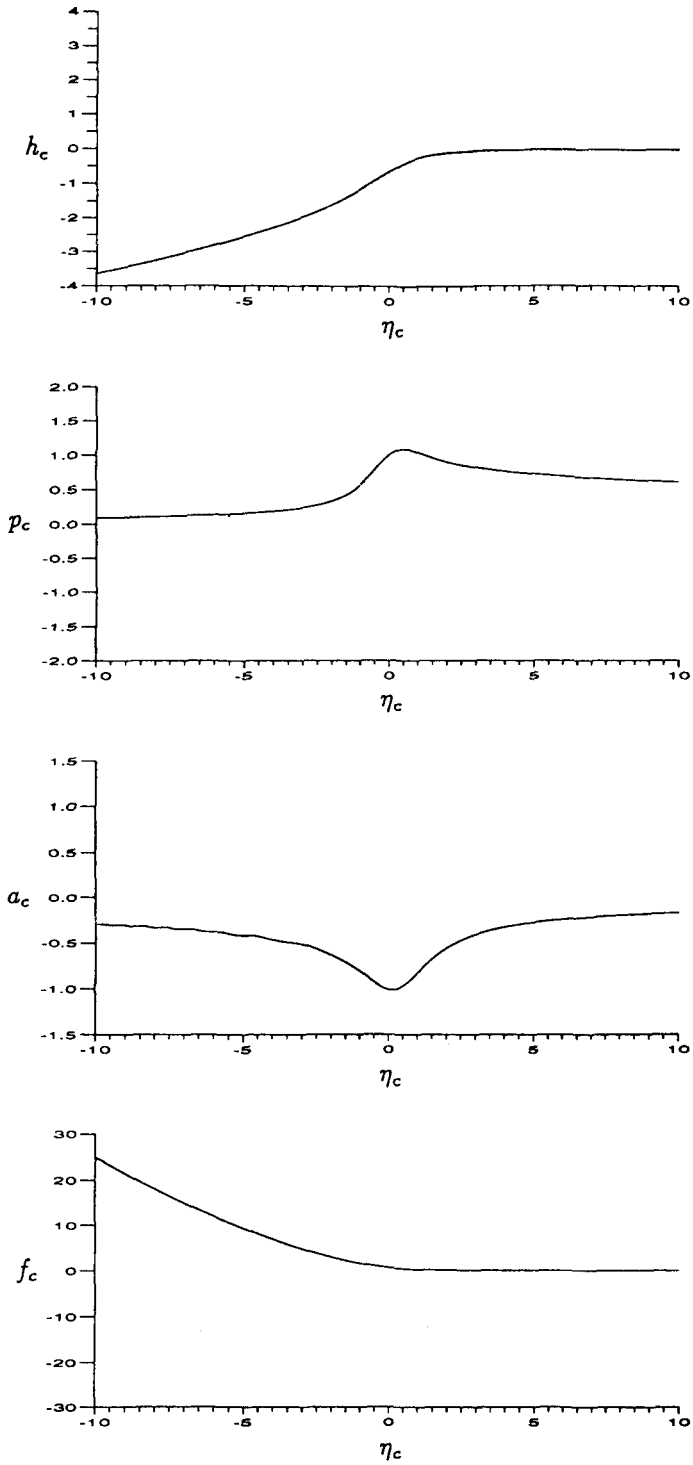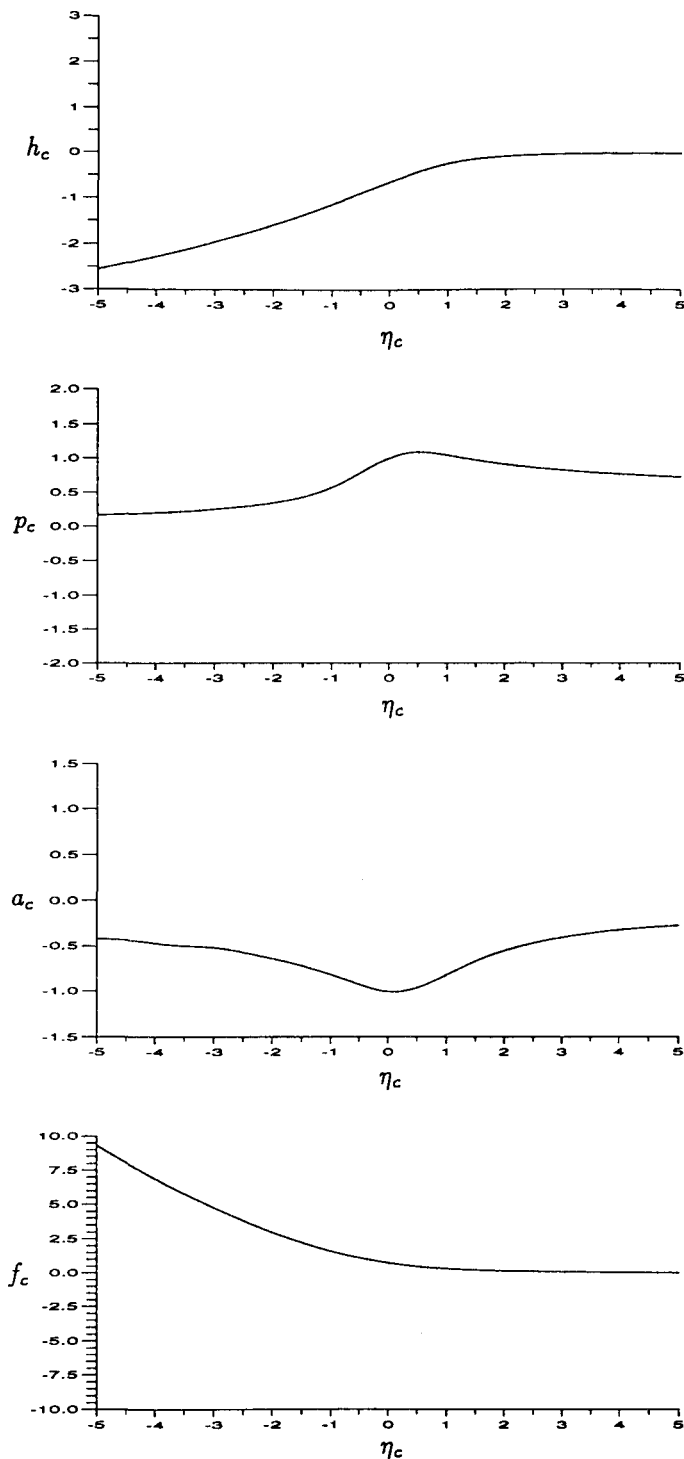
Figure 2. Solutions computed for h_c, p_c, a_c, f_c at a representative amplitude within level II, for the η_c range $[-10, 10]$. Here $\Gamma_0 = 1$. Results obtained for values of Γ_0 of $0 \cdot 8$, $1 \cdot 3$ were closely similar.

Figure 3. Solutions computed for h_c, p_c, a_c, f_c at a representative amplitude within level II, for the η_c range $[-5, 5]$. Here again $\Gamma_0 = 1$, results for $\Gamma_0 = 0.8$, 1.3 being closely similar. Compare with Fig. 2.
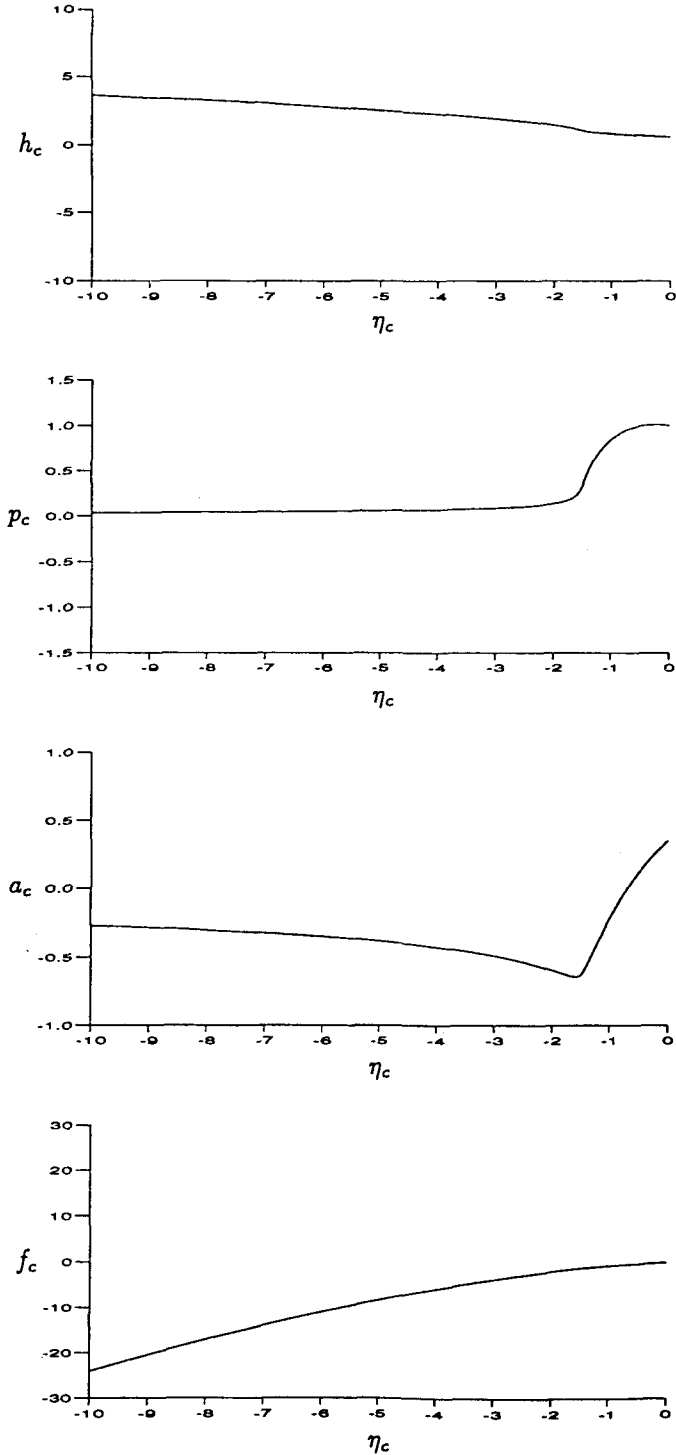
Figure 4(a). Numerical solutions for the increased amplitude response of (5.8) corresponding to the upper extreme of level II. (*a*) shows the results for negative η_c, with only the range $[-10, 0]$ being shown for clarity. (*b*), (*c*) show shooting results for positive η_c. Note the presence of a saddle point in (*b*), (*c*), *cf.* Dodia [31]; (*b*) shoots just above the saddle point and (*c*) just below it.
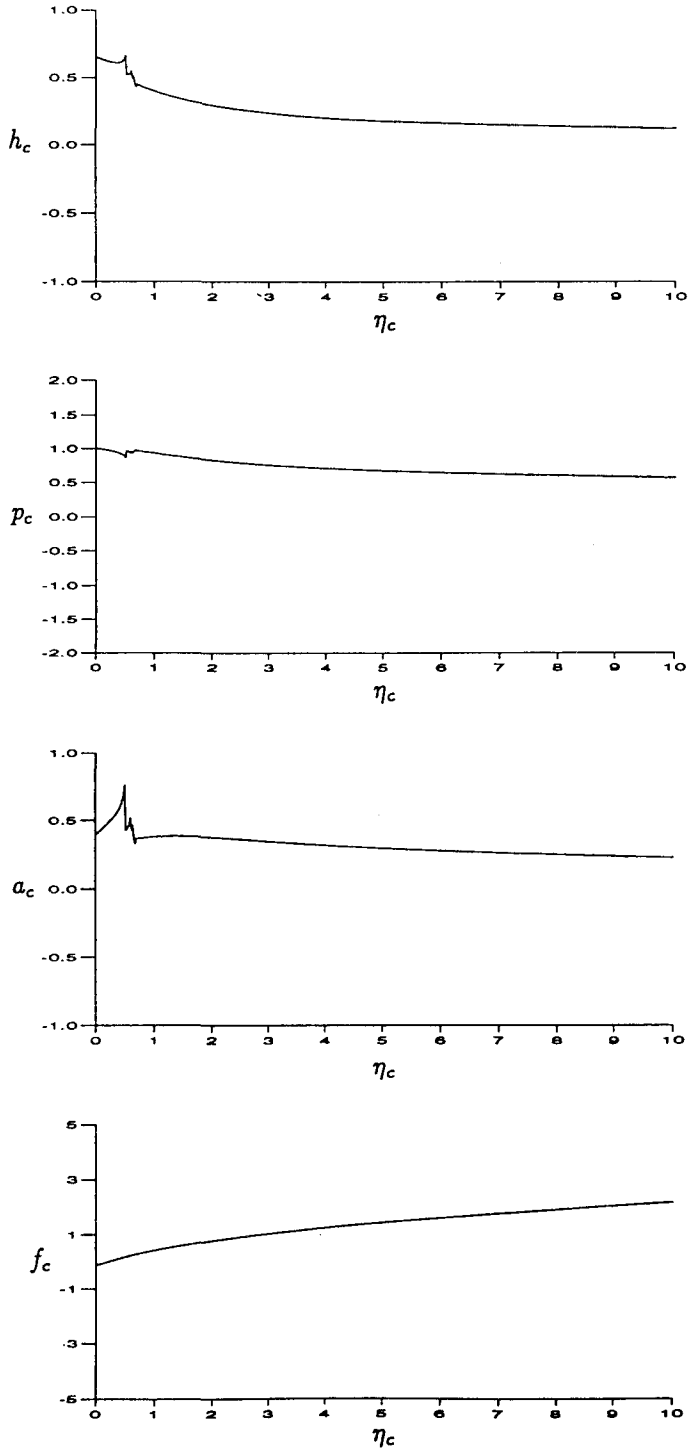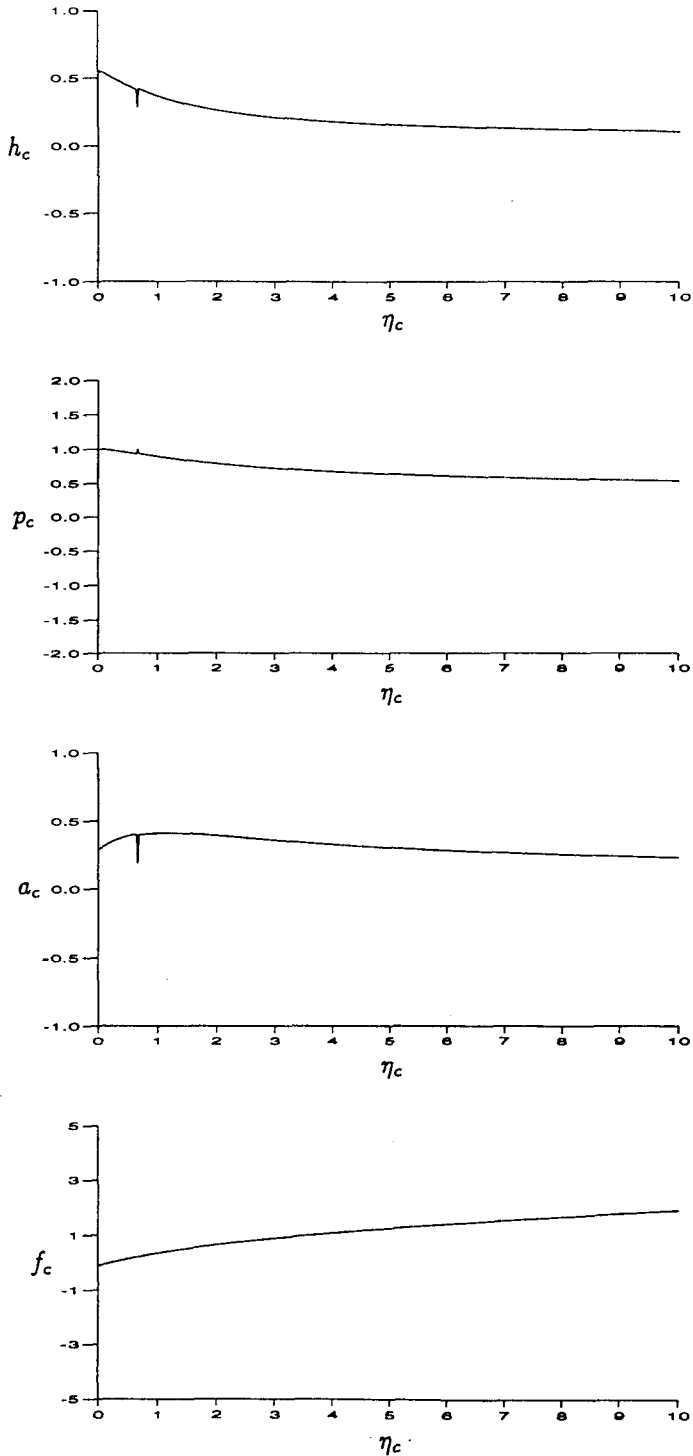
Figure 4(b).

Figure 4(*c*).

$$V = X^{(7+5n)/4}(Ev_0 + c.c.) + X^{(5+7n)/4}(Ev_{11} + c.c.) + X^{(3+9n)/4}(Ev_{21} + c.c.)$$

$$+ X^{(1+n)/2}v_m + X^{(1+11n)/4}(Ev_{31} + c.c.) + X^{(-1+3n)/2}v_{2m} + \ldots, \qquad (6.1b)$$

$$W = X^{(-1+5n)/4}(Ew_0 + c.c.) + \ldots \{\text{similar to } U\}, \qquad (6.1c)$$

$$P = X^{(3+5n)/4}(EP_0 + c.c.) + X^{(1+7n)/4}(EP_{11} + c.c.) + X^{(-1+9n)/4}(EP_{21} + c.c.)$$

$$+ X^{(-1+n)/2}P_m + X^{(-3+3n)/2}P_{2m} + \ldots, \qquad (6.1d)$$

$$A = X^{(-1+5n)/4}(EA_0 + c.c.) + \ldots \{\text{similar to } U\}. \qquad (6.1e)$$

Here $E = \exp[i(bX^2 + X^{1+n}\lambda\eta + X^{(1+3n)/2}f_1(\eta) + X^{2n}f_2(\eta) + \ldots)]$. For each new value of n, as n increases, a new term becomes significant in the phase function; thus as $n \to 1$, an infinite expansion for the phase function is produced.

Substitution of (6.1a–e) into (2.1) reveals that, to the first and second orders, the governing equations are unchanged from the case $n = 0$ of Sections 2–5. At third order, the equations differ from (3.7) only in that there are no longer any η-derivatives, as the layer-width has increased. In more detail, at first and second order the pressure-displacement relations are identical to (4.1) and (4.2) respectively. At third order the η-derivative of A_{01} in (4.3) is again lost, with no other alteration. When combined, the internal and external relations at first, second and third orders again confirm the self-consistency of the constants given in (5.1).

It is at fourth order that the current amplitude parameter n first appears in the controlling equations. The following equations holding then should be compared with (3.8):

$$\mathscr{L}(\mathbf{u}_{31}) - \mu i f_1' u_{21} + i\lambda\eta u_{11} + i f_1' w_{21} - \mu u_{0\eta} + w_{0\eta}$$

$$+ iu_0[\tfrac{1}{2}(1+3n)f_1 - n\eta f_1'] = 0, \qquad (6.2a)$$

$$\mathscr{M}(\mathbf{u}_{31}) - is\mu f_1' u_{21} + i(s-1)\lambda\eta u_{11} - s\mu u_{0\eta}$$

$$+ i(s-\tfrac{1}{2})[\tfrac{1}{2}(1+3n)f_1 - n\eta f_1']u_0 - \tfrac{1}{2}i\eta f_1' u_0 + iBA_m u_0$$

$$= i\mu f_1' P_{21} - \lambda\eta P_{11} + \mu P_{0\eta} - iP_0[\tfrac{1}{2}(1+3n)f_1 - n\eta f_1'], \qquad (6.2b)$$

$$\mathscr{N}(\mathbf{u}_{21}) - is\mu f_1' w_{21} + i(s-1)\lambda\eta w_{11} - s\mu w_{0\eta}$$

$$+ i(s-\tfrac{1}{2})[\tfrac{1}{2}(1+3n)f_1 - n\eta f_1']w_0 - \tfrac{1}{2}i\eta f_1' w_0 + iBA_m w_0$$

$$= -if_1' P_{21} - P_{0\eta}. \qquad (6.2c)$$

Note the appearance of n via the expressions in square brackets. The terms underlined are those which appeared at third order in the case where $n = 0$, and they are only present at this order if $n = 1/5$. As n continues to take larger values these terms move to even higher orders. They are important terms nonetheless and will be referred to as "moving" terms. The external relation holding at fourth order is analogous with (4.4):

$$\beta P_{31} = B^2 A_{31} - 2\mu f_1' BA_{21} + (2B\lambda\eta + \mu^2 f_1'^2 - 2\mu Bf_2')A_{11} + 2\mu iBA_{0\eta}$$

$$+ [Bf(1+3n) - 2\lambda\eta\mu f_1' - 2Bn\eta f_1' + 2\mu^2 f_1' f_2']A_0 + \tilde{\sigma}_3. \qquad (6.3)$$

Here we observe the new A_{11} term involving $f_2(\eta)$ and the appearance of n via the expression in the square brackets. Again the underlined term is present only if $n = 1/5$. The double derivative of $f_1(\eta)$ present in (4.4) is another "moving" term and is situated at fifth order if $n = 1/5$. Combining the new fourth-order internal and external relations above we obtain the first interaction equation

$$\sqrt{2}f_1'^3 + 2(1 + n)\eta f_1' - (1 + 3n)f_1 = \sqrt{3}A_m, \qquad (6.4)$$

analogous with (5.2).

The mean-flow equations must be considered next. Again there is no dependence on the parameter n at first order. At second order, however, the following equations are obtained,

$$\tfrac{1}{2}(-1 + 3n)A_m - n\eta A_{m\eta} + v_{2ms} - \mu u_{2m\eta} + w_{2m\eta} = 0, \qquad (6.5a)$$

$$-\tfrac{1}{2}[\tfrac{1}{2} + s + \tfrac{3}{2}n - 3ns]A_m + (\tfrac{1}{2}(n - 1) - ns)\eta A_{m\eta} - \mu s u_{2m\eta}$$
$$+ v_{2m} + w_0 u_{0\eta}^* - \mu u_0 u_{0\eta}^* + c.c. = 0, \qquad (6.5b)$$

$$- s\mu w_{2m\eta}^* - \mu u_0 w_{0\eta}^* + w_0 w_{0\eta}^* + c.c. = 0. \qquad (6.5c)$$

On comparing the above equations with (3.12a–c) we see that the pressure gradient forcing term is not present at this order. As at level II, there is a wall layer, in which u_{2m}, w_{2m} become unbounded like s^{-1}, but v_{2m} tends to zero. This suggests the following procedure. We first multiply (6.5b) by μ and subtract (6.5c), then substitute using (6.5a). Then by considering the result at $s = 0$ we find

$$-\tfrac{1}{4}(1 + 3n)A_m + \tfrac{1}{2}(n - 1)\eta A_{m\eta} - \mu u_0 u_{0\eta}^* + w_0 u_{0\eta}^*$$
$$+ u_0 w_{0\eta}^* - (1/\mu)w_0 w_{0\eta}^* + c.c. = 0. \qquad (6.6)$$

Substituting for u_0, w_0 and their complex conjugates, we therefore obtain the second controlling equation

$$(n - 1)\eta A_{m\eta} - \tfrac{1}{2}(1 + 3n)A_m = \frac{2(\mu B - \lambda)^2}{\mu b^2}(|P_0|^2)'. \qquad (6.7)$$

On comparing (6.7) with (5.4) (or with (5.8)) we observe the loss of the Cauchy-integral term, as expected. For all $n > 0$ this last term is of reduced significance and indeed does not appear in the main interaction equations.

In the case where $n = 0$, it is at fifth order that we find (as in Section 5) the final controlling equation necessary to describe the solution. However, as n increases and the phase contains progressively more functions $f_i(\eta)$, the final interaction equation is found at progressively higher order. For example, in the case where $n = 1/5$, it is necessary to proceed to the sixth order to reach the final equation; the fifth-order balances provide only an equation for the new phase function $f_2(\eta)$. The so-called "moving" terms discussed earlier produce the desired third interaction equation. These particular terms are present at fifth order in the case $n = 0$, at sixth order for the case $n = 1/5$ and so on. It is possible therefore to obtain the final equation, for general n, by considering solely these terms. The new phase functions that come into action do not play

a part in the final equation, and so it is not necessary to solve the equations at all preceding orders before considering the higher-order equation which contains the crucial moving terms. In this way, and again omitting the detailed working, we obtain the final equation, valid for all n such that $0 < n < 1$, as:

$$\left[\frac{3}{\sqrt{2}}f_1'^2 + (1+n)\eta\right]|P_0|' + \left[\frac{3}{\sqrt{2}}f_1'f_1'' + \tfrac{1}{4}(1-5n)\right]|P_0| = 0. \qquad (6.8)$$

This is to be compared with (5.3) which is for the lower-amplitude case $n = 0$.

The nonlinear interaction in each successive edge layer is thus described by the three equations (6.4), (6.7), (6.8) for the entire range $0 < n < 1$. It is of interest next to examine the decay of A_m and P_0 in the outer reaches of the edge layer, in particular as $\eta \to -\infty$ and the middle of the spot's trailing edge is approached. The decay is determined by the three equations above as

$$A_m \sim |\eta|^{(1+3n)/(2(n-1))}, \quad P_0 \sim |\eta|^{(3+5n)/(4(n-1))}, \quad \text{as } \eta \to -\infty. \qquad (6.9)$$

The decay here agrees with the inverse-square-root decay inferred from the factor $\hat{B}$ in (5.9) in the earlier case $n = 0$. More significantly, for higher n values it is clear that as the edge layers become wider, corresponding to increasing edge-layer amplitudes, the decay into the mid-spot trailing edge region becomes more abrupt.

We may then move on to consider finally here the behaviour of the displacement and pressure in the mid-region of the spot trailing edge, between the two edge layers (at $Z \approx \pm\mu X$) at any value of n. To this end we let the edge-layer variable $|\eta| \to O(X^{1-n})$ so that $Z - \mu X \to O(X)$, formally. The resulting orders of magnitude for the pressure and displacement are found to be independent of n, yielding the significant result that at any disturbance amplitude level between level II ($n = 0$) and level III ($n = 1$) the mean and fluctuating parts of the displacement are both $O(X^{-1})$ in the central part of the trailing edge. At these amplitude levels the equations in the central region are linear and do not fix the displacement variation explicitly, which is therefore determined by history effects and remains arbitrary. This is in agreement with our earlier work (see Smith, Dodia and Bowles [5]) in which the mid-region of the trailing edge is believed to remain linear until amplitude level III is reached, when in a relatively abrupt fashion the nonlinear effects become over-riding across the entire trailing edge (Fig. 1)

§7. *Final comments.* As far as the more immediate implications of the study are concerned, perhaps the foremost finding of the present work in the end, apart from the details, is its confirmation of the suggestions in [5] concerning the so-called amplitude level III ($n = 1$), when downstream nonlinear effects flood in from the wing-tips to cover the entire trailing-edge area. The flow structure then implied by our Section 6, as the amplitude factor $n \to 1$, is exactly as anticipated in [5] (and [30]), despite the differences and subleties associated with the join with level II, as well as with earlier lower-amplitude trailing edge properties in [29]. See in particular Section 5 of [5] for the level III structure, which is strongly nonlinear since $n = 1$. Moreover that amplitude level then

leads on even further downstream to the findings in Section 6 of [5] with respect to the spot centre. The strong more global nonlinearity met there is especially exciting, including a novel interaction, which arises on the largest scale (airfoil scale) as covered by [5]'s equations (2.1), (6.1). The nonlinear build-up inward from the spot wing-tips, in the "echelon" fashion described in Section 6, provides an explanation both of the trailing-edge response and of the calm linear region behind which is in line with some features of experiments, an explanation which no other theory seems to have provided so far.

More broadly concerning the increased physical understanding of nonlinear spots and their prediction, the length and time scales provoked in the three-dimensional spot evolution are numerous and cover a wide range as shown by the theory here and in [5, 6, 29–31]. These tend to confirm the impression of spots within spots, as in the experimental, computational and theoretical aspects reviewed by [1]–[5], particularly when the effects of viscosity are added in the form of sublayer burstings [5, 32]. Extra scales found in the present work are those of the wall layer, which helps to decide the correct mixture of the mean-flow momentum balances in Section 3, and all the new scales of phase observed in Section 6. The review in [5] also shows that the theory is tentatively in keeping with many of the principal experimental findings reviewed in [1]–[5] and references therein and while there is a great deal still to explain there are several points of fair agreement quantitatively; see also [6] on the approximate 11° spreading rate. In fact the theory here combined with [5, 6, 29, 32] is now in qualitative or quantitative agreement with experiments on major features of spots such as those listed in Section 1. See also our Fig. 1 and [6]'s Fig. 2. The above is for the boundary-layer spot, while [31] studies wall-jet and channel-flow spots.

APPENDIX A. The functions σ_n. These functions used in Section 4 are found to be given as follows for $n = 2, 3, 4$:

$$\beta\sigma_2 = -(\lambda - \mu B)(\tfrac{1}{2}\sigma_1\beta^{-1} + g_{11})f'$$
$$- \tfrac{1}{2}\{2B\lambda\bar{\eta} + (\mu^2 + 1)f'^2\}g_{01} + i(\lambda - \mu B)g'_{01}, \tag{A1}$$

$$\beta\sigma_3 = \kappa_3 - (\lambda - \mu B)f'g_{21} - \tfrac{1}{2}\{2B\lambda\bar{\eta} + (\mu^2 + 1)f'^2\}g_{11}$$
$$+ i(\lambda - \mu B)g'_{11} - \tfrac{1}{2}\{Bf - 2\mu\lambda\bar{\eta}f' - i(\mu^2 + 1)f''\}g_{01}$$
$$+ i(\mu^2 + 1)f'g'_{01}, \tag{A2}$$

$$\beta\sigma_4 = \kappa_4 - (\lambda - \mu B)f'g_{31} - \tfrac{1}{2}\{2B\lambda\bar{\eta} + (\mu^2 + 1)f'^2\}g_{21}$$
$$+ i(\lambda - \mu B)g'_{21} - \tfrac{1}{2}\{Bf - 2\mu\lambda\bar{\eta}f' - i(\mu^2 + 1)f''\}g_{11}$$
$$+ i(\mu^2 + 1)f'g'_{11} + \tfrac{1}{2}\{i(5B/2 - \lambda\mu) + \mu ff' - \lambda^2\bar{\eta}^2\}g_{01}$$
$$- \mu\lambda i\bar{\eta}g'_{01} + \tfrac{1}{2}(\mu^2 + 1)g''_{01}. \tag{A3}$$

Here

$$\beta\sigma_1 = -(\lambda - \mu B)f'g_{01}, \qquad 2\beta\kappa_2 = -(\lambda - \mu B)f'\sigma_1, \qquad (A4)$$

$$\kappa_3 = \frac{3\gamma_3}{2\beta} - \frac{f'}{2\beta}(\lambda - \mu B)\sigma_2 - \frac{\sigma_1}{4\beta}\{2B\lambda\bar{\eta} + (\mu^2 + 1)f'^2\}$$

$$+ \frac{i}{2\beta}(\lambda - \mu B)\sigma_1', \qquad (A5)$$

$$\gamma_3 = -f'(\lambda - \mu B)\kappa_2/(3\beta), \qquad (A6)$$

$$4\beta\kappa_4 = 6\gamma_4 - 2(\lambda - \mu B)f'\sigma_3 - \{2B\lambda\bar{\eta} + (\mu^2 + 1)f'^2\}\sigma_2$$

$$+ 2i(\lambda - \mu B)\sigma_2' - 2\{Bf - 2\mu f'\lambda\bar{\eta} - i(\mu^2 + 1)f''\}\sigma_1$$

$$+ 2i(\mu + 1)f'\sigma_1' - 2i\beta Bg_{01}, \qquad (A7)$$

$$6\beta\gamma_4 = -2(\lambda - \mu B)f'\kappa_3 - \{2B\lambda\bar{\eta} + (\mu^2 + 1)f'^2\}\kappa_2$$

$$+ 2i(\lambda - \mu B)\kappa_2' - 3(\lambda - \mu B)f'\gamma_3/\beta. \qquad (A8)$$

These formulae arise from the successive solutions in Section 4.

References

1. J. P. Clark, T. V. Jones and J. E. LaGraff. *J. Eng. Maths.*, 28 (1994), 1–19.
2. D. S. Henningson, A. V. Johansson and P. H. Alfredsson, *J. Eng. Maths.*, 28 (1994), 21–42.
3. A. Seifert, M. Zilberman and I. Wygnanski. *J. Eng. Maths.*, 28 (1994), 43–54.
4. F. N. Shaikh and M. Gaster. *J. Eng. Maths.*, 28 (1994), 55–71.
5. F. T. Smith, B. T. Dodia and R. G. A. Bowles. *J. Eng. Maths.*, 28 (1994), 73–91.
6. R. G. A. Bowles and F. T. Smith, *J. Fluid Mech.*, 295 (1995), 395–407.
7. H. W. Emmons. *J. aeronaut. Sci.*, 18 (1951), 490–498; see also *J. Fluid Mech.*, 9 (1963), 235–246.
8. G. B. Schubauer and P. S. Klebanoff. *NACA Rep.*, 1289 (1956).
9. M. J. Lighthill. *Introduction to boundary layer theory. Laminar boundary layers* (ed. L. Rosenhead), Ch. II (Oxford University Press, 1963).
10. H. Schlichting. *Boundary-layer theory*, 4th edn. (New York: McGraw-Hill, 1979).
11. R. E. Falco, Ch. 1.1–1.4 In *Proc. 6th Biennial Symp. Turb.* (University of Missouri-Rolla, 1979).
12. M. R. Head and P. Bandyopadhyay. *J. Fluid Mech.*, 107 (1981), 297–338.
13. A. E. Perry, T. T. Liu and E. W. Teh. *J. Fluid Mech.*, 104 (1981), 387–405.
14. F. W. Chambers and A. S. W. Thomas. *Physics Fluids*, 26 (1983), 1160–1162.
15. C. R. Smith, J. D. A. Walker, A. H. Haidari and U. Sobrun. *Phil. Trans. R. Soc. Lond.* A, 336 (1991), 131–175.
16. M. Gad-el-Hak, R. F. Blackwelder and J. J. Riley. *J. Fluid Mech.*, 110 (1981), 73–95.
17. T. Katz, A. Seifert and I. J. Wygnanski. *J. Fluid Mech.*, 221 (1990), 1–22.
18. A. V. Johansson, J. Her and J. H. Haritonidis. *J. Fluid Mech.*, 175 (1987) 119–142.
19. D. S. Henningson and P. H. Alfredson. *J. Fluid Mech.*, 178 (1987), 405–421.
20. S. K. Robinson. *Ann. Rev. Fluid Mech.*, 23 (1991), 601–639.
21. J. W. Elder. *J. Fluid Mech.*, 9 (1960), 235.
22. A. Leonard. *Springer Lecture Notes in Physics*, 136 (1981), 119–145.
23. E. T. Bullister and S. A. Orszag. *J. scient. Comput.*, 2 (1987), 263–281.
24. D. S. Henningson, P. Spalart and J. Kim. *Physics Fluids*, 30 (1987), 2914–2917.
25. D. S. Henningson and J. Kim. *J. Fluid Mech.*, 228 (1991), 183–205.
26. A. Lundbladh and A. V. Johansson. *J. Fluid Mech.*, 229 (1991), 499–516.
27. H. Fasel. In *Laminar-turbulent transition* (ed. D. Arnal and R. Michel) (Berlin: Springer, 1990).
28. U. Konzelmann and H. Fasel. *Proc. R. Aero. Soc. Meeting on Transition, Cambridge, U.K.* (1991).
29. D. J. Doorly and F. T. Smith. *J. Eng. Maths.* 26 (1992), 87–106.

30. F. T. Smith, *Phil. Trans. Roy. Soc.*, A340 (1992), 131–165.

31. B. T. Dodia, *Ph.D. thesis* (Univ. of London, 1994).

32. F. T. Smith. *Phil. Trans. Roy. Soc.*, A352 (1995), 405–424.

33. P. Hall and F. T. Smith. *J. Fluid Mech.*, 227 (1991), 641–666.

Dr. B. T. Dodia,
Department of Aeronautics,
Imperial College,
London SW7 2AZ.

Dr. R. G. A. Bowles,
Department of Mathematics,
University College London,
Gower Street,
London WC1E 6BT.

Professor F. T. Smith,
Department of Mathematics,
University College London,
Gower Street,
London WC1E 6BT.